UNIVERSITI MALAYSIA PERLIS

UniMAP

The Effect of Silver Particles on the Synthesis and Characterization of Polystyrene/Silver (Ps/Ag) Nanocomposites for Carbonaceous Materials

Jibrin Alhaji Yabagi[1*], Mohammed Isah Kimpa[2], Bello Ladan Muhammad[1], Maytham Qabel Hamzah[3,4], H. K. Abdul Kadir[5] and Mohd Arif Agam[3]

[1]*Departments of Physics, Faculty of Natural Sciences, Ibrahim Badamasi Babangida University Lapai, P.M.B 11, Lapai, Niger State, Nigeria.*
[2]*Department of Physics, School of Physical Sciences, Federal University of Technology Minna, P.M.B. 65, Minna, Niger State, Nigeria.*
[3]*Department of Physics and Chemistry, University Tun Hussein Onn Malaysia, 84600 Pagoh, Muar, Johor, Malaysia.*
[4]*Directorate of Education Al-Muthanna, Ministry of Education, Republic of Iraq.*
[5]*Department of Chemical & Petrochemical Engineering, College of Engineering, University of Anbar, Ramadi, Iraq.*

ABSTRACT

Polymer nanocomposites containing inorganic fillers like metallic particles dispersed in polymer matrices are of great interest for optical, electronics and dielectric applications. Polymer/inorganic such as polystyrene/silver nanocomposite (PS/Ag) can be manipulated through various treatments in fabricating desired material such as optical, sensors and microwave absorbance. PS/Ag nanocomposite was successfully synthesized using ex-situ mix solution technique. The composite was further investigated using Field Emission Scanning Electron Microscope and Energy Dispersive Spectroscopy (FESEM/EDS), Atomic Force Microscope (AFM), X-ray Powder Diffraction pattern (XRD), Fourier-Transform Infrared Spectroscopy (FTIR), Raman Spectroscopy and Ultraviolent-visible Spectroscopy (UV-vis). The effect of Ag particles was studied using FESEM by showing the homogenous spherical shape of the PS particle since the presence of Ag particles alters the surface morphology of the PS/Ag nanocomposites. The topographical analysis by AFM indicates a uniform surface distribution of Ag particles on the PS matrix, the root mean square and surface roughness of the PS and PS/Ag nanocomposites were found to vary with the variation of Ag particles in the composites. Furthermore, the structural pattern of the composites investigated using XRD indicates the presence of PS at $2\theta = 19.7^0$ shown by the amorphous nature of the polymers. PS/Ag nanocomposites show more peaks and pure crystalline structure of the composites. The carbonaceous structure of PS and PS/Ag nanocomposites were investigated using Raman spectroscopy which indicates the presence of the large number of carbon atoms linked together. Raman further revealed the peak at 1367 cm⁻¹ and ~1594 cm⁻¹ assigned to D-band (less ordered carbon structure) and G-band (highly oriented graphite-like structure and diamond-like carbon) within the composites.

Keyword: Polystyrene, Silver Particles, PS/Ag nanocomposites, Carbonaceous Materials, Characterization.

*Corresponding Author: jibrinyabagi@ibbu.edu.ng

1. INTRODUCTION

Most polymers used in our daily life can be produced in large quantities with low cost because polymers are unique materials that have repeating units and can be modified by either incorporating inorganic materials or manipulated with different incorporation treatment to improve their properties [1, 2]. In recent time, researchers have put forward the uses of polymer base materials for modern application in optoelectronic devices such as organic photovoltaic cells (OPVs), microwave absorbance and organic light-emitting diode (OLED) [3, 4]. Furthermore, nanoparticles (NPs) are also promising research materials due to their potential applications in nanotechnology especially transition metal nanoparticles. Additionally, transition metal nanoparticles are of continuing interest because of their fascinating catalytic, electronic and optical properties [5, 6]. One of the major benefits of using polymer-based as electronic materials is the possibility to introduce inorganic nanoparticles to modify the polymer structure toward desired properties [7]. In the area of chemistry and material science, polystyrene is usually used due to its essential physical properties such as lightweight and flexibility compared to other matrices, like ceramics and metals which are one of the most widely used as matrix material in composites for high-end applications. Polystyrene (PS) matrix has the potential to improved production rates, lower the cost, and processability [8]. In order to improve the strength, toughness, electrical conductivity and thermal stability of polystyrene particles, various nanofillers are added to the prepared desired polystyrene nanocomposites based on different applications [9].

The addition of a small amount of electrically conductive nanofiller such as gold (Au), silver (Ag) and copper (Cu) nanoparticles can increase the electrical conductivity of polymer materials by orders of magnitudes. The nanofillers with other interesting properties may be added to customize and extend other functions of polymers [10]. Moreover, the main problem associated with this research comprises the preparation and incorporation of silver particles in the matrix of polystyrene particles [11]. The well-known nanoparticles that are usually used for coating in the polystyrene matrix are Au and Ag as they show similar optical properties within the visible region [12]. But Ag particles emerge as the promising candidate in this modern-day technology due to its high reactivity than Au. Flexibility and low density of polystyrene particles make them suitable for nanoparticles encapsulation process, thereby preventing the separation of the composite to achieve the desired nanostructure. Until now, PS has been the most considerable thermoplastic polymer as it has strong adsorption ability, higher surface area, high transparency and biocompatibility which make PS suitable for medical and optical application [13]. In recent time, many research published on the preparation of Ag particles disperse in the polymer matrix through in-situ polymerization, melt blending method, and solution mixing technique [14-16]. It has been quite tricky to disperse nanoparticles into the polymer homogeneously due to viscous nature and agglomeration behaviour of the polymer with Ag particle. However, solution mixing provides homogeneous composites that can be used for many applications [14].

In the present work, polystyrene containing different wt% of Ag nanoparticles was prepared through ex-situ chemical synthesis method. In the first stage, Ag NPs was prepared using chemicals reduction methods and further disperse into the PS matrix to form PS/Ag nanocomposites. Furthermore, the effect Ag particles dispersed in PS matrix was studied based on morphological and structural patterns, chemical bonding and optical analysis using Field Emission Scanning Microscopy (FESEM), Atomic Force Microscopy (AFM), Energy Dispersive X-ray Spectroscopy (EDS), X-ray Powder Diffraction (XRD) Fourier Transformation Infrared spectra (FTIR), Raman Spectroscopy and Ultraviolet (UV-vis).

2. MATERIALS, METHOD AND APPARATUS

The raw materials used in synthesizing silver particles (AgPs) and polystyrene/silver (PS/Ag) nanocomposites are silver nitrate (AgNO$_3$ with a molecular mass of 169.87 g/mol 99.8% purity) (Sigma-Aldrich), sodium borohydride (NaBH$_4$ with a molecular mass of 37.83 g/mol 98.5%) (R & M), polyvinylpyrrolidone (PVP with a molecular mass of 160,000 g/mol 98.9%) (R & M) and microsphere dispersion of 500 nm polystyrene nanosphere commercial polystyrene (Sigma-Aldrich), Silicon wafer (100 single crystal orientations, p-doped, resistivity 6.0-9.0 ohm.cm), diamond cutter, cuvettes (quartz and glass) 10 mm, hydrogen peroxide (H$_2$O$_2$) 30% v/v (R&M), and saturated hydrochloric acid (HCl) 35% v/v (Sigma-Aldrich).

2.1 Synthesis of Silver Particles

Silver particles were synthesized via a chemical reduction method and incorporated in PS in a different ratio in order to study its effect. The experimental procedure was modified from Mavani & Shah [15]. Silver particles were synthesized using PVP as capping and NaBH$_4$ as reduction agents via the chemical method. A series of experiments were performed by varying the concentration of silver nitrate while the stabilizer and reductions remain constant in order to obtain perfect silver colloid. The colloidal solutions are obtained by mixing 0.4 M aqueous solutions of silver nitrate and 0.1% of PVP in the presence of stirring for 10 minutes using a magnetic stirrer to get a homogeneous solution. PVP was added to silver nitrate due to the formation of hydrophobic domains that surround metal particles and protect them against agglomeration. These were followed by adding the appropriate amount of 0.01 M sodium borohydride under vigorous stirring for 20 minutes. The transparent bright yellow colour was observed, immediately due to the formation of silver colloids where sodium borohydride is expected to reduce all silver ions even at the highest precursor concentration because it is expected to supply an excess of electrons for reduction. However, the general procedure for Ag particles preparation is summaries in Figure 1 below.
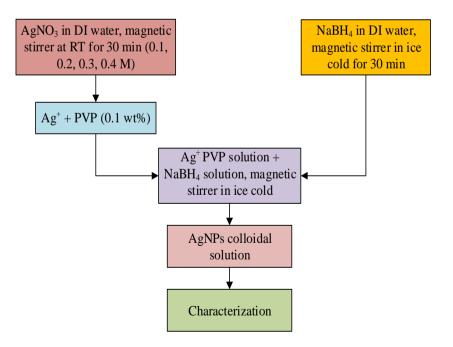

Figure 1. Schematic representing the process of the Ag particles synthesized by chemical reduction method.

2.2 Preparation of PS/Ag Nanocomposite

Nanocomposites of PS/Ag are prepared using ex-situ solution mix technique and sonication methods. The experimental procedure was modified from [16]. This method involves the dispersion of Ag particles in the polymer and the solution thereby interlocking the filler within the matrix of the polymer. The colloidal solution of Ag particles with concentration 0.3 M was incorporated into PS colloidal in a different proportion volume ratio between 1:2, 1:4 and 1:8 v/v in order to investigate the effect of Ag particles in the newly formed PS/Ag nanocomposite. After adding Ag particles, the nanocomposite was subjected to vortex homogenizer machine for 2 minutes, regular mixing at high-speed rotation before introduced to high-frequency ultrasonic agitation for 45 minutes vibration to for better dispersing of Ag particles into PS matrix. Figure 2 shows the illustration of the formation mechanism of PS/Ag nanocomposites.
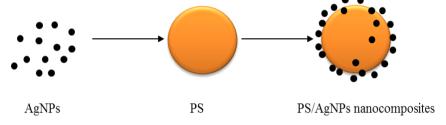
AgNPs   PS   PS/AgNPs nanocomposites

Figure 2. Schematic diagram of the formation of PS/Ag nanocomposites.

2.3 Surface Morphology Analysis of PS/Ag Nanocomposites

The effect of Ag particle on the morphology of PS/Ag nanocomposites are explained by FESEM analysis. The dispersion condition of Ag particles in the PS matrix directly correlates with its effectiveness in enhancing the performances of nanocomposites. The interaction between Ag particles and the PS matrix was investigated by FESEM and shown in Figure 3 (a-d). The particles exhibit a regular spherical shape and homogeneously distributed which are the characteristic of conventional PS particles. The morphological results revealed in Figure 3 (b-d) show well-arranged hexagonal and closely packed structure for PS and nanocomposites with 1:2, 1:4 and 1:8v/v of Ag particles. However, the incorporation of Ag particles shows the influence of the nanoparticles on the surface morphology of the composites materials (see Figure 3 (b-d)). Further addition of more Ag particles into the PS matrix shows a rough morphology compared to PS alone. PS/Ag nanocomposites were obtained through solution mixing and morphology of the composites shows more agglomeration with the addition of Ag particles in the composites. The morphology analysis of the composites indicates that the PS particles contain porous/void part of the PS matrix, while the composites form a cluster thereby making energetic interfacial interaction within the PS matrix and disperse Ag particles. This may be due to the interaction of the aromatic π-electrons of polystyrene and free electrons of metal nanoparticles which also causes an improvement in phase transition temperature accordingly [17]. The surface morphology was significantly changed after adding the nanoparticles.
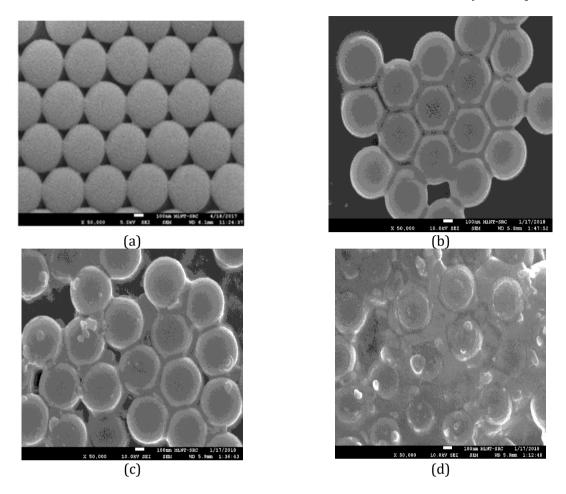
Figure 3. FESEM images of: (a) PS, (b) 1:2 v/v, (c) 1:4 v/v, and (d) 1:8 v/v PS/Ag nanocomposites (50K magnification).

Furthermore, the Ag particles presence in the PS matrix was dispersed particularly in the composites contain 1:8, thereby indicating void area within the image of PS matrix shows a certain aggregation of Ag particles which leads to some interaction between OH group in the Ag and OH in PS particles within the boundary of the PS matrix. This result was supported by FTIR, AFM and Raman Spectroscopy. In addition, the result also suggests that an increase of Ag particles in the sample makes the composites more aggregated [18].

However, the chemical bonding analysis study by Raman Spectroscopy and FTIR revealed that there is a clear interaction between PS matrix and Ag particles which shows a strong bond in the composites with the addition of Ag nanoparticles. Similar results were observed with another polymer film such as PMMA [19] and PVA [20] incorporated with Ag particles. The authors in their separate studies observed a well-distributed and uniform shape of silver particles in PVA films stabilized with PGA and PMMA. Similarly, Wang *et al*. [13] also observed that the use of poly (dopamine) as a chelating agent for silver ions to prepare PS/Ag composite microspheres. The interaction between the silver particle and PS matrix was enhanced by the aggregation in the PS/Ag nanocomposites, which was probably due to shell irregularity in the composites materials.

2.4 Elemental Composition Analysis of PS/Ag Nanocomposite

The elemental composition of PS/Ag nanocomposites was investigated by Energy Dispersive X-ray Spectroscopy (EDS). EDS composition was carried out to verify the presence of Ag particles element incorporated into PS. X-ray mapping capability (also known as elemental mapping) of

the EDS technique to observe elemental distribution in the nanocomposite films. In x-ray mapping, positions of specific elements emitting characteristic x-rays within an inspection field can be indicated by a specific colour. A silicon drift detector of size 20 mm² was fitted to the FESEM for EDX analysis. The results of EDS are summarized in Table 1, which indicates chemical compositions of the films. Figure 4 (a-d) depict the EDS spectrum of PS and PS/Ag nanocomposite at different ratio of Ag particles. Figure 4 (a) shows PS with the two kinds of atoms existed in the scanned sample which is carbon (C) and silicon (Si) with the energy of 0.277 keV and 1.65 keV, respectively. Figure 4 (b-d) show the EDS spectrum of PS/Ag nanocomposite with four kinds of atoms, carbon element (C), silicon (Si), silver (Ag) and gold (Au) with the energy of about 0.277 keV, 1.65 keV, 2.98 keV at accelerating voltage of 5-10 keV. Based on the results, it was confirmed the Ag particles content increase from 13.67, 17.03 to 47.37 wt% for 1:2, 1:4 and 1:8 PS/Ag nanocomposite. It can also be noted that the silver particles intensity increase as the Ag particles ratio increase in the structure, where the carbon K-line intensity decrease with a higher content of Ag particles [19, 18]. This analysis is also supported by FTIR spectra indicating that higher intense of C-H vibrating stretching in the region of the PS/Ag nanocomposites significantly decrease as described in Figure 8.
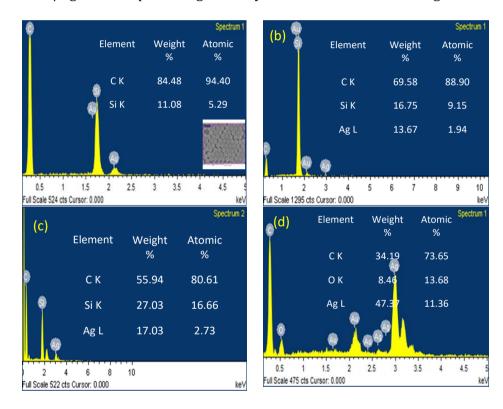

Figure 4. EDS spectrum of (a) PS (b) 1:2 v/v (c) 1:4 v/v (d) 1:8 v/v PS/Ag nanocomposites.

Table 1 Elemental composition of PS and PS/Ag nanocomposites

Sample	Element	Weight %	Atomic %
	C	84.48	94.40
PS	Si	11.08	5.29
	Au	4.45	0.30
	C	69.58	88.90
PS/Ag 1:2	Si	16.75	9.15
	Ag	13.67	1.94
	C	55.94	80.61
PS/Ag 1:4	Si	27.03	16.66
	Ag	17.03	2.73
	C	34.19	73.68

PS/Ag 1:8	O	8.46	13.68
	Ag	47.37	11.36
	Au	9.98	1.31

These results are consistent with chemical composition data which showed the variation of carbon-related peaks are due to the addition of more Ag particles concentration in the composites. These findings agree with what was found by Zhao *et al.* [21]. However, their report indicates the energies bond at 1.0, 0.85 and 3.4 keV assigned to O, C and Ag respectively. The presence of carbon element in the EDS spectrum is related to PS. The distribution of elements in the prepared PS/Ag nanocomposites can be assessed by EDS-mapping 2D projected elemental maps shown in Figure 5 (a-b) which demonstrate the uniform distribution of C element and Ag element in the prepared PS/Ag nanocomposites. Detection of C element is attributed to polystyrene. This is evident from the chemical structure of polystyrene. Further, the Ag element is detected because of the incorporation of Ag particles to the polystyrene. These maps reveal that C and Ag are the elemental constituents of PS/Ag nanocomposite film. The elemental map of silver (Ag), as seen in Figure 5 (d), shows a fairly uniform distribution of green dots/segments. This qualitatively suggests a homogeneous dispersion of silver particles in the polystyrene matrix.
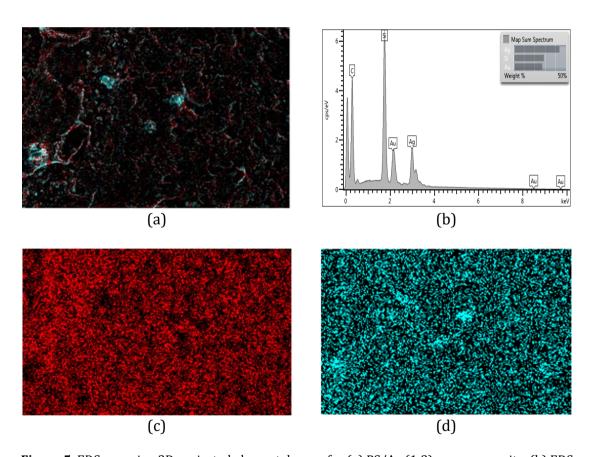

(a)

(b)

(c)

(d)

Figure 5. EDS-mapping 2D projected elemental maps for (a) PS/Ag (1:2) nanocomposite, (b) EDS spectrum, (c) carbon (C), and (d) silver (Ag).

2.5 Topography Analysis of PS/Ag Nanocomposites

The surface topography and roughness of irradiated PS/Ag nanocomposite were investigated using Atomic Force Microscopy (AFM). AFM images of the PS and PS/Ag nanocomposite films are shown in Figure 6 (a-d). PS shows the uniform distribution and uniform dispersion of Ag particles into the PS matrix as described in Figure 6 (b-d) and the smooth surface morphology of

films are clearly shown from AFM images. The average grain size, root mean square and roughness are estimated and tabulated in Table 2. The images of PS/Ag nanocomposite is rougher compared to PS alone, the increase in roughness is due to Ag particles content.

Table 2 Statistical parameters for the PS and PS/Ag nanocomposites

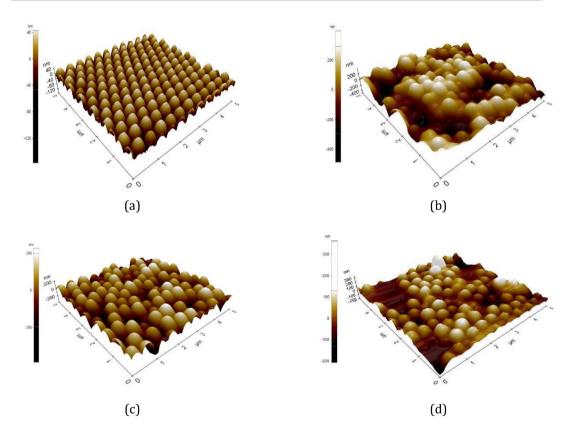| Statistical	PS	PS/Ag 1:2	PS/Ag 1:4	PS/Ag 1:8
Average grain size (nm)	139.0	287.3	229.3	174.5
R_a	20.4	123.7	81.8	50.5
RMS R_q (nm)	23.8	149.3	100.3	65.6
Skewness R_{sk}	0.29	0.24	0.47	-0.68
Kurtosis R_{ku}	2.39	2.38	2.87	5.53

(a)

(b)

(c)

(d)

Figure 6. 3D AFM images obtained for (a) PS, (b) 1:2 v/v, (c) 1:4 v/v, and (d) 1:8 v/v PS/Ag nanocomposites.

Root means square and surface roughness are found to be 20.4, 123.7, 81.8 and 50.5 nm for PS, 1:2, 1:4 and 1:8 PS/Ag nanocomposites films, respectively. The increase in surface roughness of polymer nanocomposites will enhance light absorption in photodetector applications [22].

2.6 Structural Analysis of PS/Ag Nanocomposites

The XRD pattern ascribed change in crystallite size and average intermolecular spacing after Ag particles were introduced into the PS matrix. XRD pattern can offer valuable information on the interaction processes in PS/Ag nanocomposite. Figure 7 (a-d) show the XRD pattern of PS and PS/Ag nanocomposites. Figure 7 (a) shows the diffraction pattern of PS indicates around 2θ value of 19.7° showing the amorphous phase where a similar peak was observed by Ali *et al*. (2017). Figure 7 (b) depicts that new peaks at 2θ values of 19.5°, 29.6°, 35.4° and 56.1° are generated while the intensity of peak at 2θ value of 19.5° increased after incorporated Ag

particles. On account of Ag particles incorporated into PS, the H-bond of PS chains could break and molecular chains are free to rotate due to covalent bonding [23].
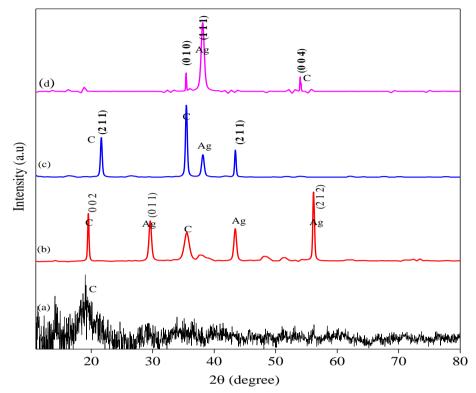

Figure 7. X-ray diffraction patterns of (a) PS, (b) 1:2 v/v, (c) 1:4 v/v, and (d) 1:8 v/v PS/Ag nanocomposites.

The peaks at 2θ values of 29.6°, 35.4° and 56.1° correspond to *h k l* parameters (*011*), (*010*), (*112*) and (*212*). The peak observed at 56.1° might be due to some disorder created in the matrix after incorporating Ag particles. Further, the increase in the silver content into the PS matrix, new characteristic peaks appeared at 2θ values of 35.5°, 38.1°, 43.4°, indicated by the pronounced peak of the PS nanocomposite. The XRD spectra showed the diffraction peaks of (*211*), (*010*), *(111)* and *(004),* which were all observed in each peak [24]. The peak of PS at the 2θ value of 19.5° is observed to shift up by 2.1° in PS incorporated Ag particles for 1:4 samples. This shift might be due to changes in d-spacing values of the corresponding planes. The intensity of diffracted patterns for samples 1:4 and 1:8 has increased after the incorporating process. It may be due to increasing the number of PS chains after incorporated Ag particles [25]. The values of FWHM and d-spacing of such peaks are tabulated in Table 3.

The crystal structures of the samples were determined by the powder XRD technique as described by [26]. The crystalline sizes calculated are listed in Table 3. A typical XRD pattern of polystyrene shifted to 2θ value of 21.6° due to the Ag particles ratio. These results indicate the structure of materials is hexagonal and PS/Ag nanocomposites were obtained. A similar result was observed by Gavade, Singh, & Singh, [27]. The authors observed that the peak intensity of the XRD pattern of the sample increase, while the FWHM decreases and the crystalline structure as well as particles size increase over the addition of Ag particles in the sample.

Table 3 Structural parameters of PS/Ag nanocomposite

Samples	2θ(º)	FWHM	d-spacing (Å)	h k l	Average Crystallite size (Å)	Lattice parameters a (Å)
1:2	19.5	0.2362	4.54726	002	6.0	4.27
	29.6	0.4723	3.01998	011	3.0	
	35.4	0.9446	2.52776	010	1.5	
	43.4	0.4723	2.08563	112	3.1	
	56.1	0.2362	1.63876	212	6.6	
1:4	21.6	0.3149	4.10820	211	4.5	4.09
	35.5	0.3149	2.53213	010	4.6	
	38.1	0.4723	2.35972	111	3.1	
	43.4	0.2362	2.08429	112	6.3	
1:8	35.4	0.0900	2.53289	010	16.1	4.09
	38.1	0.5760	2.36001	111	2.5	
	53.9	0.0900	1.69753	044	17.3	

2.7 Chemical Bonding Analysis of PS/Ag Nanocomposites

In order to understand the formation mechanism of PS/Ag nanocomposites and interaction behaviour between Ag particles and PS matrix, FTIR spectra analysis was performed to confirm the molecular structure of PS/Ag nanocomposites. Figure 8 (a-d) shows FTIR spectra of PS and incorporation of PS with Ag particles of at a different ratio (1:2, 1:4 and 1:8 v/v). All the possible bond formation between the PS matrix and silver particles added to the PS molecule/atoms were investigated by FTIR spectra. The result shows that there are slight broadening and decrease of intensity due to certain absorption bond located at 1490 cm^{-1}, 1601 cm^{-1} and 3061-2850 cm^{-1} and subsequently the bond disappears at 1601 cm^{-1} and 1460-1447 cm^{-1}, visibly indicating the high interaction between Ag particles and H and O atoms in the PS chain [28]. Although, FTIR of synthesized Ag particles before incorporated into polystyrene as described by [29] showed a band at 1300 cm^{-1} and 887 cm^{-1} which are assigned to the –CH stretching vibration of paraffin was affected by PS molecules.

However, decoupling the bond between O-H and C-H are due to decrease of the intensity and bonds broadening at 1644 cm^{-1}, these were assigned to the formation of bonds between O and H atoms with Ag particles. The bonds disappear at 1384 cm^{-1} suggesting chemical conjugation of PS molecular chain with Ag particles [18]. The variation of the intensity of the bonds at 1490 cm^{-1}, 1447 cm^{-1}, 1062 cm^{-1} and 1031 cm^{-1} shows the chemical interaction between Ag particles and matrix of PS molecules. The above results are in agreement with composition analysis data discuss in Figure 7 and Table 3, which indicate lower carbon peaks with a low concentration of silver particles in the composites. The bands are observed and functional group of PS and PS/Ag nanocomposites are summarized in Table 4. FTIR spectrum of the PS has characteristic bands at 3061 cm^{-1}, 3027 cm^{-1}, 2924 cm^{-1}, 2850 cm^{-1} and 1610 cm^{-1}, that are associated with aliphatic C–H and –CH$_2$ and aromatic C=C vibrating stretching, respectively [31-34 ;12]. The vibration mode at 3420 cm^{-1}, 3022 cm^{-1}, 2924 cm^{-1} 2846 cm^{-1}, 1602 cm^{-1}, 1490 cm^{-1} and 1447 cm^{-1} spectral are affected due to presence of Ag particles as nanofiller by comparing the intensities between spectra of PS and PS/Ag nanocomposites. This result supports the suggestion that the introduction of Ag particles increased the degree of crystallinity of PS which was consistent with the XRD results.
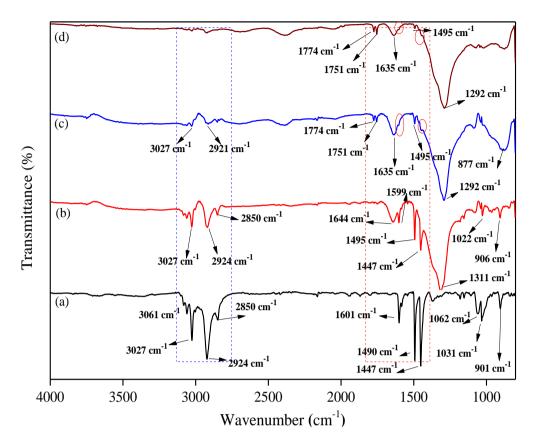
Figure 8. FTIR spectra for (a) PS (b) 1:2 v/v (c) 1:4 v/v (d) 1:8 v/v PS/Ag nanocomposites.

Table 4 Function group identification of PS and PS/Ag nanocomposite from FTIR analysis

PS	PS/Ag 1:2	PS/Ag 1:4	PS/Ag 1:8	Assignments
3061	3061	-	-	Aromatic
3027	3027	3027	-	C-H
2924	2924	2921	-	stretching vibration
2850	2850	2850	-	
-	-	1774	1774	
-	-	1751	1751	
-	1635	1635	1635	
1601	1599	1601	1601	Aromatic C=C
1490	1495	1495	1495	stretching vibration
1447	1447	1447	1447	
-	1311	1292	1292	
1062		-	-	Aromatic C–H
1031	1022	-	-	deformation
901	906	877	-	vibration

The vibration of the methyl groups was observed due to the appearance of bonds at 1292 and 877 cm^{-1}. The most intense peaks were observed at 3022 cm^{-1}, 2924 cm^{-1} 2846 cm^{-1}, 1602 cm^{-1}, 1490 cm^{-1} and 1447 cm^{-1}, thereby indicating the loss of water molecule in the sample and scission of the methyl group while the acrylate carboxylic bond was observed at 1292 cm^{-1}. The bending mode of CH methyl groups was observed at 1447 cm^{-1}. The two bands at 1644 and 1292 cm^{-1} are ascribed to the aromatic C=C stretching vibration [35]. This reduction of intensities is attributed to the increased amount of Ag particles within the mixture that push PS

chains far apart which may lead to hydrogen bonds weak [11]. As the concentration of Ag particles increases in PS, additional peaks were observed at 1774 cm^{-1}, 1751 cm$^{-1,}$ and 1535 cm^{-1}. The new bands may be correlated likewise with defects induced by the charge transfer reaction between PS chain and Ag particles.

FTIR results of the PS/Ag nanocomposites also demonstrated a change in aromatic PS regions that shifted to lower wavenumbers and FTIR results were compared with PS. The study indicates that π-π stacking was due to shifting of acrylate interaction which was assigned to Ag particles contribution to stabilized the metal surface in the composites materials [11]. Furthermore, the FTIR analysis results also suggest that the transfer of electrons was attributed due to π-π bonding interaction between Ag particles and PS atoms. These results were further supported by Ali *et al*. [18] experimental analysis. Their findings show the vibrating stretching of bonds at 3420 cm^{-1}, 2930 cm^{-1}, 1650 cm^{-1}, 1440 cm^{-1}, 1370 cm^{-1} and 1025 cm^{-1}. Some bonds appear at higher wavenumber as compared to the IR analysis of PS/PVP and Ag/PS/PVP composites. Increase of Ag particles in the composites sample leads to the shifting of bonds in the polymer chain, thereby reducing the intensity of hydrogen bonding to a higher wavelength [11].

2.8 Chemical Structure Analysis Of PS/Ag Nanocomposites

The most widely used instrument for investigating carbon base materials and obtaining information on phase and structural disorder is known as Raman spectroscopy [36]. The configuration of C-C bonding analysis was investigated by Raman scattering and the result show the major peak at 1580 cm^{-1} assigned to G-band in the mono-crystalline graphite indicating the Raman active mode due to vibrating stretching mode of C=C band in the hexagonal plane, while the D-band structure observed at 1350 cm^{-1} was due to disorder of defective graphite or micro-crystalline structure [39].

Figure 9 presents the Raman analysis of the PS/Ag nanocomposites and PS matrix, the carbonaceous structure of the polymer observed due to higher content of carbon atoms within the polymer matrix [37]. Usually, the carbonaceous structure observed at G and D-band which assigned to sp^3 and sp^2 vibrating stretching of carbon modes, while the intensity ratio (I_D/I_G) was used to estimate the disorder on the materials reported by Ding *et al*. [40]. The carbonaceous nature of this materials was observed at ~1367 cm^{-1} and ~1594 cm^{-1} suggesting the D-band (less ordered carbon structure) and G-band (highly oriented graphite-like structure and diamond-like carbon) [41]. However, Figure 9 denies the presence of such a peak in the PS (plot (a)).
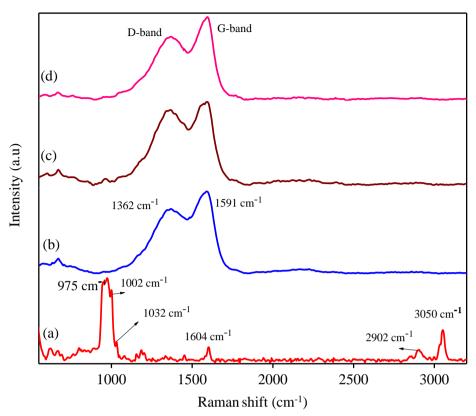
Figure 9. Raman spectra of PS/Ag nanocomposites at different ratio of Ag (a) PS (b) 1:2 v/v (c) 1:4 v/v (d) 1:8 v/v.

It can be seen that the increase in the intensities of the G-band and FWHM are affected due to the increase in Ag particles. The peaks in the G-band are slightly high; this could be the incorporation of high ratio Ag particles, which may be due to the confinement of electrons in short chains [42]. The values of the I_D/I_G ratio would be used to measure the sp^2 phase size oriented in rings. The structural disorder of the G-band peaks was highly sensitive to the full width at half maximum (FWHM), which usually occur from bond length and bond angle distortion. The free defected cluster of the G-band peak found to be small due to the small nature of the FWHM [43]. In any cluster, higher bond length and bond angle are due to higher FWHM which leads to more content of sp^3 and a higher bond gap can be observed [44]. Moreover, the bond found at 1352 cm^{-1} is attributed to the D-band of the carbonaceous materials which are observed in the PS/Ag nanocomposites. The bond appears at 1540 cm^{-1} in the Raman spectra of the composites is due to the effect of the addition of Ag particles in composites materials. The D and G-band spectra were enhanced due to chemical bonding formation between Ag particles and PS matrix has been reported in the FTIR result showing in Figure 8, which is significantly equal to what was observed in FWHM and the intensity ratio (I_D/I_G). Gaussian fitting was employed to investigate over-dependence of sp^2/sp^3 on I_D/I_G ratio and FWHM as they have different information. Figure 10 shows the Gaussian fitting of the Raman analysis of PS/Ag nanocomposites at a different ratio of Ag particles content. Gaussian fitting was used to determine the positions of the bands along with their intensity ratio (I_D/I_G) and FWHM of the bands. The ratio of I_D/I_G for PS/Ag nanocomposites is presented in Table 5.
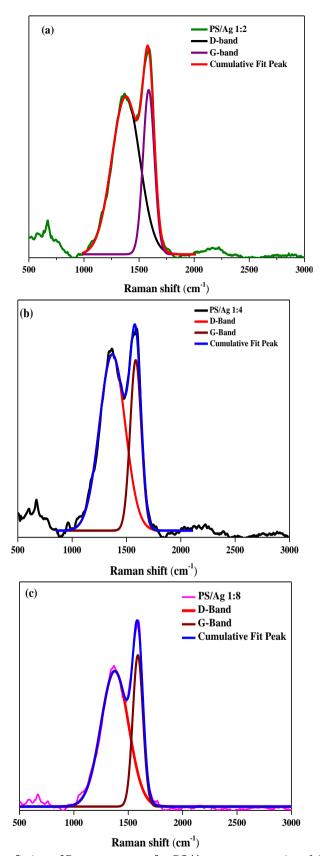
Figure 10. Gaussian curve fitting of Raman spectra for PS/Ag nanocomposites (a) 1:2 (b) 1:4 (c) 1:8 v/v.

Table 5 Raman peak parameters for PS/Ag nanocomposites

Samples PS/Ag	D-band			G-band			(I_D/I_G)
	Position (cm^{-1})	FHWM (cm^{-1})	Peak height	Position (cm^{-1})	FWHM (cm^{-1})	Peak height	
1:2	1367.9	298.1	21993.6	1591.1	120.9	28029.2	0.7
1:4	1362.4	278.4	19740.6	1590.6	120.6	21887.5	0.9
1:8	1369.4	299.4	31712.8	1595.0	110.0	41342.6	0.8

The peak fitting results show that the intensities ratio of D band and G band for Raman spectra are in the range of 0.7 – 0.9, which are the range values for diamond-like carbon (DLC). The I_D/I_G value for the 1:2 was found to be 0.8 and increases with the increased amount of Ag particles. These revealed the formation of the carbonaceous structure with a small content of the sp^2 C–C bonding. Furthermore, the value of intensity ratio I_D/I_G increases from 0.7 to 0.9 as a result of the increased in Ag particles content. The increase in the I_D/I_G ratio indicates an increase in sp^2 content [45]. FWHM of G-band for all samples indicate a significant change with an increase in the amount of Ag particles. FWHM of G-band for 1:2 decreased with increasing Ag particles where value for 1:8 is significantly lower than corresponding values for 1:2 samples indicating that inclusion of silver particles in the PS matrix which resulted in more sp^2 rich due to line width and I_D/I_G intensity ratio that varies depending on the structure of the carbon. Thus, PS/Ag (1:8) is rich in sp^2 bonded carbon with smaller bond angle disorder when the sample contained a higher amount of Ag particles into the PS matrix. Thus, Ag particles into the PS matrix would lead to structural change and render the PS matrix to be more graphitic in nature [46]. These results are also consistent with the characteristics shown in the FTIR spectra.

2.9 Optical Transmittance Analysis Of PS/Ag Nanocomposites

Optical transmittance spectra are normally determined by UV-Visible spectroscopy. The optical transmittance spectra of PS/Ag nanocomposites are recorded in a range of 300-1000 nm wavelength via UV-1800 Shimadzu spectrophotometer as described by Ghanipour [25]. Figure 11 shows optical transmittance plot of PS/Ag nanocomposite PS, 1:2 v/v, 1:4 v/v, and 1:8 v/v. It was observed that the spectra of samples with Ag particles (1:4 and 1:8 v/v) has higher transmittance of 46.92% and 55.39% at a wavelength of 350 nm, respectively. This could be due to the high content of Ag particles and strong interaction of conduction electrons of Ag with photons of light which results in high transmittance implying that Ag particles are much transparent in the visible region, while PS and 1:2 v/v have lower transmittance of 19.87% and 22.291%. The comparison between the prepared PS/Ag nanocomposites and PS particles revealed the absorption characteristic of the noble-metal particles determined by collective electron oscillations and the surface plasma resonance.
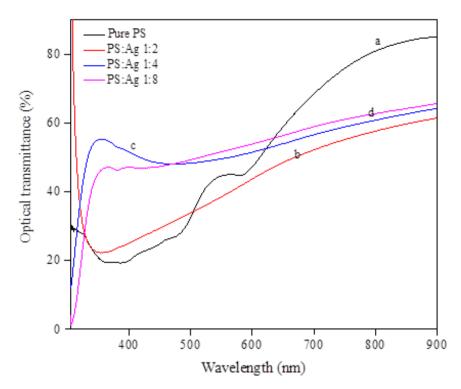
Figure 11. Plot of optical transmittance against wavelength for PS/Ag nanocomposite at (a) PS, (b) 1:2 v/v, (b) 1:4 v/v, and (c) 1:8 v/v.

3. CONCLUSION

In summary, Ag particles have been successfully prepared by chemical reduction method as described above and the consequence of Ag particles on PS was studied by FESEM/EDS, UV-vis, AFM, XRD, FTIR and Raman spectroscopy. The effect of Ag particles incorporated into PS on morphologies, structural, optical and chemical properties was investigated. Morphologies of PS/Ag nanocomposites revealed the extent of filler dispersion. FTIR analysis indicated a slight decrease in the intensity and broadening of absorption and disappearance of bands as Ag particles were incorporated into PS. The decrease in intensity and broadening of bands suggest decoupling between C-H and O-H bonds due to bond formation of Ag particles with O and H atoms and disappearance of the band also indicates chemical conjugation of Ag particles with the molecules of PS chains. Raman spectra revealed information regarding the DLC films structure due to its ability to distinguish between sp^2 and sp^3 bonds type. In general, the results of Raman consist of a broad peak at ~1367.89 cm^{-1} (D-band) and ~1594.96 cm^{-1} (G-band). XRD pattern of incorporated Ag particles into PS revealed that the structure of PS changed from amorphous phase to crystalline phase by creating new peaks as the content of Ag particles increases. UV–visible studies indicated chemical bond formation between PS and Ag particles causing an increase in the band from 2.0 eV to 2.88 eV as the Ag content increases.

ACKNOWLEDGMENT

Nanotechnology-Shamsuddin Research Centre (Mint-SRC) Universiti Tun Hussein Onn Malaysia (UTHM) for technical assistance and characterization analysis.

REFERENCES

[1] Hadi, A. J., Abdulkadir, H. K., Hadi, G. J., Yusoh, K. B., & Hasany, S. F. Mechanical and Thermal Properties of the Waste Low and High Density Polyethylene-nanoclay Composites. Oriental Journal of Chemistry **34**, 2 (2018) 1069-1077.

[2] Z. Deng *et al.,* "Synthesis of PS/Ag nanocomposite spheres with catalytic and antibacterial activities," ACS Appl. Mater. Interfaces, **4** (2012) 5625–5632.

[3] Abdul Kadir, H. K., Jaya, H., Noriman, N. Z., Dahham, O. S., Mazelan, A. H., Latip, N. A., & Aini, A. K. The Effects of Phthalic Anhydride On R-Hdpe/Eva/Cff Composites: Tensile and Physical Properties. In IOP Conference Series: Materials Science and Engineering **454** (2018) 012191.

[4] M. A. Nassar & A. M. Youssef, "Mechanical and antibacterial properties of recycled carton paper coated by PS/Ag nanocomposites for packaging," Carbohydr. Polym. **89**, (2012) 269–274.

[5] J. Kuljanin-Jakovljević, M. Marinović-Cincović, Z. Stojanović, A. Krklješ, N. D. Abazović, and M. I. Čomor, "Thermal degradation kinetics of polystyrene/cadmium sulfide composites," Polym. Degrad. Stab. **94** (2009) 891–897.

[6] Y. Cong *et al.,* "Mussel-inspired polydopamine coating as a versatile platform for synthesizing polystyrene/Ag nanocomposite particles with enhanced antibacterial activities," J. Mater. Chem. B **2** (2014) 3450–3461.

[7] Jaya, H., Abdul Kadir, H. K., Noriman, N. Z., Omar, S. D., Mazelan, A. H., Latip, N. A., & Aini, A. K. The Influences of Chicken Feather Loading on Tensile and Physical Properties of R-Hdpe/Eva/Cff Composites. In IOP Conference Series: Materials Science and Engineering **454** (2018) 012190.

[8] A. A. Mostafa, H. Oudadesse, M. M. H. El Sayed, G. Kamal, M. Kamel, and E. Foad, "Kinetic evaluation study on the bioactivity of silver doped hydroxyapatite-polyvinyl alcohol nanocomposites," J. Biomed. Mater. Res. - Part A **102** (2014) 4609–4615.

[9] D. Wu, X. Ge, Y. Huang, Z. Zhang, and Q. Ye, "γ-Radiation synthesis of silver-polystyrene and cadmium sulfide-polystyrene nanocomposite microspheres," Mater. Lett. **57** (2003) 3549–3553.

[10] I. Y. Jeon & J. B. Baek, "Nanocomposites derived from polymers and inorganic nanoparticles," Materials (Basel). **3** (2010) 3654–3674.

[11] E. H. Alsharaeh, "Polystyrene-poly(methylmethacrylate) silver nanocomposites: Significant modification of the thermal and electrical properties by microwave irradiation," Materials (Basel). **9** (2016) 6-18.

[12] J. A. Yabagi, M. I. Kimpa, M. N. Muhammad, K. I. Uthaman, E. Zaidi, & M. A. Agam, "Structural Transformation of Polystyrene Nanosphere Produce Positive and Negative Resists by Controlled Laser Exposure," Adv. Sci. Lett. **23** (2017) 6613–6617.

[13] W. Wang, Y. Jiang, S. Wen, L. Liu, & L. Zhang, "Preparation and characterization of polystyrene/Ag core-shell microspheres -A bio-inspired poly(dopamine) approach," J. Colloid Interface Sci. **368** (2012) 241–249.

[14] J. S. Noh, "Conductive elastomers for stretchable electronics, sensors and energy harvesters," Polymers (Basel) **8** (2016) 4-12.

[15] K. Mavani & M. Shah, "Synthesis of Silver Nanoparticles by using Sodium Borohydride as a Reducing Agent," Int. J. Eng. Res. Technol. **2** (2013) 1–5.

[16] Z. I. Takai, M. K. Mustafa, & S. Asman, "Preparation of high performance conductive polyaniline magnetite (PANI/Fe3O4) Nanocomposites by Sol-Gel Method," Asian J. Chem., **30** (2018) 122-130.

[17] Z. I. Takai *et al.,* "Gamma ray and FTIR studies in zinc doped lead borate glasses for radiation shielding application," Mater. Res., **22** (2018) 1-9.

[18] I. Ali, M. R. Akl, G. A. Meligi, & T. A. Saleh, "Silver nanoparticles embedded in polystyrene-polyvinyl pyrrolidone nanocomposites using ??-ray irradiation: Physico-chemical properties," Results Phys., **7** (2017) 1319–1328.

[19] M. N. Siddiqui, H. H. Redhwi, E. Vakalopoulou, I. Tsagkalias, M. D. Ioannidou, and D. S. Achilias, "Synthesis, characterization and reaction kinetics of PMMA/silver nanocomposites prepared via in situ radical polymerization," Eur. Polym. J. **72** (2015) 256–269.

[20] D. G. Yu, W. C. Lin, C. H. Lin, L. M. Chang, & M. C. Yang, "An in situ reduction method for preparing silver/poly (vinyl alcohol) nanocomposite as surface-enhanced Raman scattering (SERS)-active substrates," Mater. Chem. Phys. **101** (2007) 93–98.

[21] W. Zhao, Q. Zhang, H. Zhang, & J. Zhang, "Preparation of PS/Ag microspheres and its application in microwave absorbing coating," J. Alloys Compd. **473** (2009) 206–211.

[22] R. A. Ismail, N. J. Almashhadani, & R. H. Sadik, "Preparation and properties of polystyrene incorporated with gold and silver nanoparticles for optoelectronic applications," Appl. Nanosci. **7** (2017) 109–116.

[23] R. P. Chahal, S. Mahendia, A. K. Tomar, & S. Kumar, "γ-Irradiated PVA/Ag nanocomposite films: Materials for optical applications," J. Alloys Compd, 538 (2012) 212–219.

[24] A. Mirzaei, K. Janghorban, B. Hashemi, M. Bonyani, S. G. Leonardi, & G. Neri, "Characterization and optical studies of PVP-capped silver nanoparticles," J. Nanostructure Chem. **7** (2017) 37–46.

[25] M. Ghanipour & D. Dorranian, "Effect of Ag-Nanoparticles Doped in Polyvinyl Alcohol on the Structural and Optical Properties of PVA Films," J. Nanomater. **10** (2013) 201-218.

[26] J. Mohammed *et al.,* "Tuning the dielectric and optical properties of Pr–Co–substituted calcium copper titanate for electronics applications," J. Phys. Chem. Solids **126** (2019) 226-235.

[27] C. Gavade, N. L. Singh, A. Sharma, P. K. Khanna, & F. Singh, "The effect of SHI irradiation on structural, thermal and dielectric properties of a silver nanoparticle-embedded polystyrene matrix," Radiat. Eff. Defects Solids **166** (2011**)** 585–591.

[28] K. Sharma, R. P. Chahal, S. Mahendia, A. K. Tomar, & S. Kumar, "Optical behaviour of swift heavy ions irradiated poly (vinyl alcohol) films," Radiat. Eff. Defects Solids **168** (2013) 378–384.

[29] E. H. Alsharaeh, "Polystyrene-poly (methyl methacrylate) silver nanocomposites: Significant modification of the thermal and electrical properties by microwave irradiation," Materials (Basel) **9** (2016) 6-15.

[30] J. A. Yabagi, M. I. Kimpa, M. N. Muhammad, S. Bin, E. Zaidi, & M. A. Agam, "The effect of gamma irradiation on chemical, morphology and optical properties of polystyrene nanosphere at various exposure time," IOP Conf. Ser. Mater. Sci. Eng. **298** (2018) 1–10.

[31] P. J. Wibawa, H. Saim, M. A. Agam, & H. Nur, "Design, preparation and characterization of polystyrene nanospheres based-porous structure towards UV-vis and infrared light absorption," Phys. Procedia **22** (2011) 524–531.

[32] M. U. Mustafa, M. A. Agam, N. R. Md Juremi, F. Mohamad, P. J. Wibawa, & A. H. Ali, "Physical and chemical changes of polystyrene nanospheres irradiated with laser," AIP Conf. Proc. **1347** (2011) 67–71.

[33] U. O. Aroke & U. A. El-Nafaty, "XRF, XRD and FTIR Properties and Characterization of HDTMA-Br Surface Modified Organo-Kaolinite Clay," Int. J. Emerg. Technol. Adv. Eng. **4** (2014) 817–825.

[34] L. Wang, L. Yan, P. Zhao, Y. Torimoto, M. Sadakata, & Q. Li, "Surface modification of polystyrene with atomic oxygen radical anions-dissolved solution," Appl. Surf. Sci. **254** (2008) 4191–4200.

[35] J. M. Lee, Y. D. Jun, D. W. Kim, Y. H. Lee, & S. G. Oh, "Effects of PVP on the formation of silver-polystyrene heterogeneous nanocomposite particles in novel preparation route involving polyol process: Molecular weight and concentration of PVP," Mater. Chem. Phys. **114** (2009) 549–555.

[36] Jaya, H., Noriman, N. Z., AbdulKadir, H. K., Dahham, O. S., Muhammad, N., Latip, N. A., & Aini, A. K., (December). The Effects of Wood Sawdust Loading on Tensile and Physical Properties of Up/Pf/Wsd Composites. In IOP Conference Series: Materials Science and Engineering **454** (2018) 012193.

[37] O. Akhavan, R. Azimirad, H. T. Gholizadeh, & F. Ghorbani, "Hydrogen-rich water for green reduction of graphene oxide suspensions," Int. J. Hydrogen Energy **40** (2015) 5553–5560.

[38] T. Roch, V. Weihnacht, & H. Scheibe, "Direct Laser Interference Patterning of tetrahedral amorphous carbon films for tribological applications," Diam. Relat. Mater **33** (2013) 20–26.

[39] S. Adhikari, M. S. Kayastha, D. C. Ghimire, H. R. Aryal, S. Adhikary, & T. Takeuchi, "Improved Photovoltaic Properties of Heterojunction Carbon Based Solar Cell," J. Surf. Eng. Mater. Adv. Technol. **3** (2013) 178–183.

[40] Y. H. Ding, P. Zhang, Q. Zhuo, H. M. Ren, Z. M. Yang, & Y. Jiang, "A green approach to the synthesis of reduced graphene oxide nanosheets under UV irradiation," Nanotechnology **22** (2011) 5.

[41] T. A. Saleh, M. M. Al-Shalalfeh, & A. A. Al-Saadi, "Graphene Dendrimer-stabilized silver nanoparticles for detection of methimazole using Surface-enhanced Raman scattering with computational assignment," Sci. Rep. **6** (2016) 32-45.

[42] H. Zhang, J. L. Endrino, & A. Anders, "Comparative surface and nano-tribological characteristics of nanocomposite diamond-like carbon thin films doped by silver," Appl. Surf. Sci. **255** (2008) 2551–2556.

[43] S. F. Ahmed, M. Moon, & K. Lee, "Effect of silver doping on optical property of diamond like carbon films," Thin Solid Films **517** (2009) 4035–4038.

[44] D. M. Chipara, J. Macossay, A. V. R. Ybarra, A. C. Chipara, T. M. Eubanks, & M. Chipara, "Raman spectroscopy of polystyrene nanofibers—Multiwalled carbon nanotubes composites," Appl. Surf. Sci. **275** (2013) 23–27.

[45] A. Tamulevic, A. Vasiliauskas, D. Virganavic, & S. Tamulevic, "Structuring of DLC: Ag nanocomposite thin films employing plasma chemical etching and ion sputtering," Nucl. Instruments Methods Phys. Res. B **341** (2014) 1–6.

[46] R. P. Chahal, S. Mahendia, A. K. Tomar, & S. Kumar, "SHI irradiated PVA/Ag nanocomposites and possibility of UV blocking," Opt. Mater. (Amst). **52** (2016) 237–241.